# Temperature Influences on State and Parameter Estimation Based on a Dual Kalman Filter

Christian Campestrini*, Georg Walder†, Andreas Jossen* and Markus Lienkamp†
*Institute for Electrical Energy Storage Technology, Technische Universität München, Email: c.campestrini@tum.de
†Institute of Automotive Technology, Technische Universität München, Email: walder@ftm.mw.tum.de

***Abstract*—The temperature dependency of a Dual Kalman Filter (DKF) is shown. For this purpose a validation process is developed to show the behaviour of the filter at various cell temperatures (5 °C, 25 °C, and 35 °C). Additionally, the validation process reveals some unresolved problems such as the behaviour during constant voltage periods. The behaviour of the DKF is compared to experimental data. The state estimator predicts the state of charge (SOC) with an accuracy of 1.5 % within the investigated temperature range. Furthermore, the state estimator is able to reproduce the observed characteristics of the ohmic resistance ($R_{dc1s}$) of the equivalent circuit model (ECM).**

## I. Introduction

Nowadays, electric mobility gains sufficiently importance. Due to the reduced range compared to a vehicle equipped with a conventional combustion engine battery electrical vehicles (BEV) and hybrid electrical vehicles (HEV) still play a minor role in today's mobility. With a reliable state determination of the built in battery system, the usable amount of energy can be raised and, hence, the range can be increased. In literature, numerous algorithms for the state estimation can be found [1, 2, 3, 4, 5]. However, these algorithms are mostly tested within the laboratory scale at predefined conditions. The shortcomings of these algorithms are often not shown. Therefore, this paper presents a validation method to test state estimators for the mentioned shortcomings. Here, the Dual Kalman Filter is investigated. The focus lies on the temperature dependency of relevant state parameters of the battery and, consequently, on the high requirements of the filter. In chapter II the ECM used is presented and the identification process of the reference parameters is shown. In chapter III the DKF used here is explained [6]. The validation method is shown and some problems of the filter are revealed in chapter IV. The results are presented and discussed in chapter VI.

## II. Battery modelling

To describe the behaviour of batteries an ECM can be applied. The most frequently used ECM is a simple model, which consists of a direct voltage source, a serial resistor and one or more RC-terms. With an increasing number of RC-terms, the accuracy of the model increases as well. However, this leads to a higher complexity and, consequently, to an increased demand on the computational effort (e.g. battery management system, BMS). Due to the limited computational power that can be implemented on a BMS, different ECMs were compared in [7] to find a compromise between accuracy and computational time. The resulting ECM is shown in figure 1.

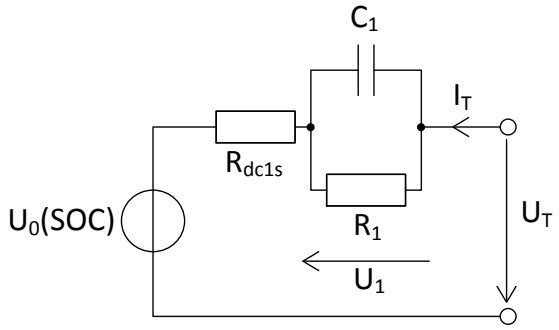


Fig. 1. The equivalent circuit model with one RC-term

$U_0$ corresponds to the SOC dependent open circuit voltage (OCV). Due to the current sample rate of 1 s, $R_{dc1s}$ corresponds to the serial ohmic resistance and to the charge transfer effects. $R_1$ and $C_1$ corresponds to the elements of the RC-term. $U_1$ is the voltage drop by the RC-term and contains diffusion effects, $U_T$ and $I_T$ corresponds to the terminal voltage and current. Applying the mesh rule, the following set of equations can be found to describe the states in the time domain.

$$\begin{bmatrix} \dot{U}_1(t) \\ \dot{SOC}(t) \end{bmatrix} = \begin{bmatrix} -\frac{1}{R_1 C_1} & 0 \\ 0 & 0 \end{bmatrix} \begin{bmatrix} U_1(t) \\ SOC(t) \end{bmatrix} + \begin{bmatrix} \frac{1}{C_1} \\ \frac{1}{C_N} \end{bmatrix} I_T(t) \quad (1)$$

$$U_T(t) = U_0(SOC(t)) + R_{dc1s} \cdot I_T(t) + \dot{U}_1(t) \quad (2)$$

$C_N$ is the capacity of the cell. The exact derivation of the equations can be found in [6]. After the discretisation of the ECM the DKF can be implemented.

The parameters of the model can be identified by measuring the voltage response of a battery as a result of current pulses over the entire SOC range (5 % SOC steps). In figure 2 the voltage response as a result of a current pulse is shown. The voltage drop between P1 and P2 is used to calculate the resistor $R_{dc1s}$. The following voltage drop between P2 and P3 is a result of the diffusion effects. After the end of the pulse, the cell relaxes.

The pulses were performed at 5 °C, 25 °C and 35 °C every 5 % ΔSOC. Applying this method, the measured parameters can be compared to the estimation using the DKF as a function of SOC and temperature.

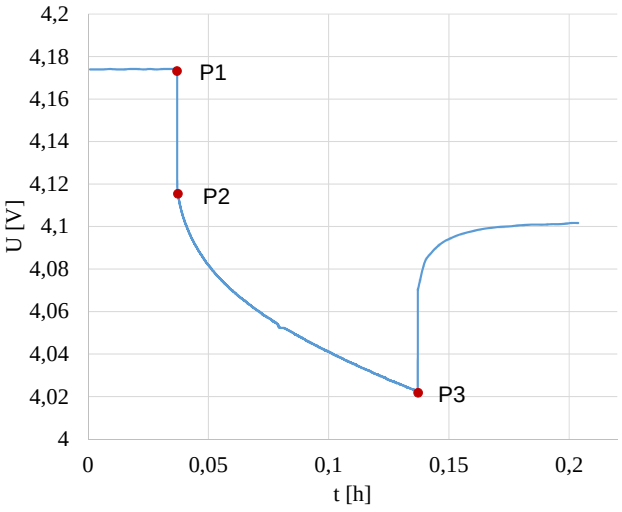


Fig. 2. Voltage response as a result of a current pulse and the characteristic points

## III. The Dual Kalman Filter

Within this paper, the investigations are carried out using the DKF which was introduced in [6]. This implementation has already shown good agreement of the estimated states of the battery as well as the parameters of the ECM with measured data. This filter is a combination of a Linear Kalman Filter which estimates the states $U_1$ and $SOC$ and an Extended Kalman Filter which estimates the parameters $C_N$ (cell capacity), $R_{dc1s}$, $R_1$ and $C_1$.

Referring to the findings of [6] further optimisation is shown here. The resulting filter structure can be found in figure 3.

The dual filter structure contains an update and a correction of the state and parameter estimation. Thereby, the expected states are updated with the calculation of the state space formulation in equation 3.

Due to the fact that the state space formulation does not exist for the parameters of the ECM, an update is not possible and the adaptation of the parameters has to be done in the correction. This results in the fact that the input $\hat{w}_k^-$ for the correction is the parameter $\hat{w}_{k-1}^+$ from the previous step (figure 3). For a dynamic adaptation of the parameters it is vital to consider the process noise of the parameters themselves.

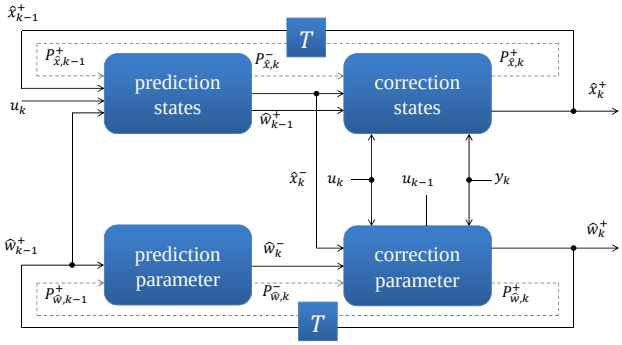


Fig. 3. The structure of the DKF

| | |
|---|---|
| $\hat{x}_{k-1}^+$ | estimated state of the step before |
| $\hat{x}_k^-$ | updated state of the actual step |
| $\hat{x}_k^+$ | corrected state of the actual step |
| $P_{\hat{x}_{k-1}}^+$ | state error covariance of the step before |
| $P_{\hat{x}_k}^-$ | updated state error covariance of the actual step |
| $P_{\hat{x}_k}^+$ | corrected state error covariance of the actual step |
| $P_{\hat{w}_{k-1}}^+$ | parameter error covariance of the step before |
| $P_{\hat{w}_k}^-$ | updated parameter error covariance of the actual step |
| $P_{\hat{w}_k}^+$ | corrected parameter error covariance of the actual step |
| $u_k$ | actual input |
| $u_{k-1}$ | input of the step before |
| $y_k$ | measured output |
| T | time transformation |

A first coupling of the two filters is implemented at the beginning of each cycle $k$ given the fact that the parameters are the input for the state and parameter estimator. A second coupling is achieved in the correction, as the updated state $\hat{x}_k^-$ is also necessary for the parameter correction [6].

The parameter $R_{dc1s}$ can be found only in the output equation $\hat{y}_k$ but not in the equations of the state vector $\hat{x}_k$. Hence, $R_{dc1s}$ can be removed from the parameter estimator and can be added to the state estimator. Due to this, the performance of the resistor $R_{dc1s}$ estimation and the stability of the filter could be increased.

The resulting discrete state space formulation is presented in equation 3 and 4.

$$\underline{\hat{x}}_k = \Phi_k \cdot \underline{\hat{x}}_{k-1} + \underline{b}_k \cdot u_k + \underline{v}_k \tag{3}$$

$$\hat{y}_k = \underline{h}_k \cdot \underline{\hat{x}}_k + n_k \tag{4}$$

with

$$\underline{\hat{x}}_k = \begin{bmatrix} U_{1_k} \\ SOC_k \\ R_{dc1s_k} \end{bmatrix} \tag{5}$$

$$\Phi_k = \begin{bmatrix} e^{-\frac{T_s}{R_1 C_1}} & 0 & 0 \\ 0 & 1 & 0 \\ 0 & 0 & 1 \end{bmatrix} \tag{6}$$

$$\underline{b}_k = \begin{bmatrix} R_1 \left(1 - e^{\frac{T_s}{R_1 C_1}}\right) \\ \frac{T_s}{C_N} \\ 0 \end{bmatrix} \tag{7}$$

The output vector $\underline{h}_k$ is calculated to

$$\underline{h}_k = \begin{bmatrix} 1 \\ \frac{U_0(\hat{x}_{2_k}^-)}{\hat{x}_{2_k}^-} \\ I_k \end{bmatrix} \tag{8}$$

The variables $\underline{v}_k$ and $\underline{n}_k$ represent an independent, zero–mean, Gaussian process and measurement noise. The equations for the calculation of the linear state estimator based on [6] are shown in table I.

| description | equation |
|---|---|
| prediction states | $\underline{\hat{x}}_k^- = \Phi_k \cdot \underline{\hat{x}}_{k-1}^+ + \underline{b}_k \cdot u_k$ |
| measurement update | $\hat{y}_k = \underline{h}_k \cdot \hat{x}_k^-$ |
| prediction error covariance | $\mathrm{P}_k^- = \Phi_k \cdot \mathrm{P}_{k-1}^+ \cdot \Phi_k^T + \mathrm{Q}_k$ |
| Kalman gain | $\mathrm{K}_k = \mathrm{P}_k^- \cdot \underline{h}_k^T \cdot (\underline{h}_k \cdot \mathrm{P}_k^- \cdot \underline{h}_k^T + \mathrm{R}_k)$ |
| correction states | $\underline{\hat{x}}_k^+ = \underline{\hat{x}}_k^- + \mathrm{K}_k(y_k - \hat{y}_k)$ |
| correction error covariance | $\mathrm{P}_k^+ = (\mathrm{I} - \mathrm{K}_k \cdot \underline{h}_k)\mathrm{P}_k^-$ |

TABLE I. EQUATIONS FOR THE LINEAR KALMAN FILTER

The matrices $\mathrm{Q_k}$ and $\mathrm{R_k}$ are the process and measurement noise matrices, I is the identity matrix.

The parameters $C_N$, $R_1$ and $C_1$ are estimated with the Extended Kalman Filter shown in table II.

| description | equation |
|---|---|
| state space formulation | $\underline{x}_k = f(\underline{x}_{k-1}, \underline{w}_k, u_k) + \underline{v}_k$ <br> $\underline{y}_k = g(\underline{x}_k, u_k) + \underline{n}_k$ |
| prediction parameter | $\underline{\hat{w}}_k^- = \underline{\hat{w}}_{k-1}^+$ |
| prediction error covariance | $\mathrm{P}_{w_k}^- = \mathrm{P}_{w_{k-1}}^+ + \mathrm{Q}_{w_k}$ |
| Kalman gain | $\mathrm{K}_{w_k} = \mathrm{P}_{w_k}^- \cdot \mathrm{H}_w^T \cdot (\mathrm{H}_w \cdot \mathrm{P}_{w_k}^- \cdot \mathrm{H}_w^T + \mathrm{R}_{w_k})$ |
| correction parameter | $\underline{\hat{w}}_k = \underline{w}_k^- + \mathrm{K}_{w_k}(y_k - \hat{y}_k)$ |
| correction error covariance | $\mathrm{P}_{w_k}^+ = (\mathrm{I} - \mathrm{K}_{w_k} \cdot \mathrm{H}_w)\mathrm{P}_{w_k}^-$ |

TABLE II. EQUATIONS FOR THE EXTENDED KALMAN FILTER

$\mathrm{Q}_w$ and $\mathrm{R}_w$ are the process and measurement noise matrices for the parameter estimator. For the implementation the Jakobi matrix of the matrix $\mathrm{H}_w$ is needed. For this purpose the partial derivation has to be calculated [8]. The formulation of the partial derivation is:

$$\begin{aligned} \mathrm{H}_{w,k} &= \frac{\mathrm{d}g(\underline{\hat{x}}_k^-, u_k)}{\mathrm{d}\underline{\hat{w}}_k^-} \\ \frac{\mathrm{d}g(\underline{\hat{x}}_k^-, u_k)}{\mathrm{d}\underline{\hat{w}}_k^-} &= \frac{\delta g(\underline{\hat{x}}_k^-, u_k)}{\delta \underline{\hat{x}}_k^-} \frac{\mathrm{d}\underline{\hat{x}}_k^-}{\mathrm{d}\underline{\hat{w}}_k^-} \\ \frac{\mathrm{d}\underline{\hat{x}}_k^-}{\mathrm{d}\underline{\hat{w}}_k^-} &= \frac{\delta f(\underline{\hat{x}}_{k-1}^+, u_{k-1}, \underline{\hat{w}}_k^-)}{\delta \underline{\hat{w}}_k^-} \\ &\quad + \frac{\delta f(\underline{\hat{x}}_{k-1}^+, u_{k-1}, \underline{\hat{w}}_k^-)}{\delta \underline{\hat{x}}_{k-1}^-} \frac{\mathrm{d}\underline{\hat{x}}_{k-1}^+}{\mathrm{d}\underline{\hat{w}}_k^-} \end{aligned} \tag{9}$$

## IV. THE VALIDATION METHOD

Within the literature various algorithms for the state estimation can be found which are validated by applying different methods. Due to this, the comparison of the algorithms is not easy. Furthermore, shortcomings of the estimators are often not considered within the validation process. Therefore, in this chapter the problems of the DKF are shown and a feasible validation process is presented.

### A. Determination of the reference state of charge

An important issue of the validation is the determination of the reference SOC to compare the estimated SOC with a reliable value. A common method to measure the reference SOC is the Ah-counter. For this issue, mostly the same current sensor is applied which is also used for the Kalman Filter. Hence, the accuracy of the estimation is determined by using the same sensor signal as for the reference. So, a profound evaluation considering the accuracy of the state estimation is not possible. Consequently, a more accurate validation is needed. This can be achieved by including a second current sensor with a higher accuracy [3, 6, 9].

By the determination of the reference SOC with a Ah-counter the finite sample rate causes an error during dynamic current curves (green area in figure 4 A). This error increases with an increase of time. A more accurate possibility is a rest discharge at the end of the test. Due to the constant current discharge the accumulated errors because of the finite sample rate can be neglected (figure 4 B). This issue is mandatory during long term tests.

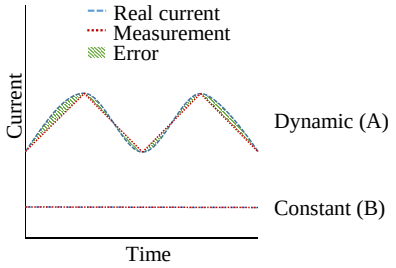


Fig. 4. Comparison of the error due to the finite sample rate during a dynamic current discharge and a constant current discharge

### B. Influence of the temperature

The parameters of a battery are dependent on the temperature. Furthermore the OCV changes with temperature depending of the chemistry and SOC [10]. Xing et al. [3] shows the influence of the temperature depending OCV of a Lithium-Iron-Phosphate (LFP) cell to the state estimation with a KF. To resolve this problem different OCVs at different temperatures were implemented in the battery model. The OCV of the cell (NMC) used in this paper has a small dependency of the temperature. Due to this the variation of the OCV with the temperature is neglected here and only the OCV at 25 °C is used. The self-heating of the cell during the driving cylce is lower than 1 °C and thereby neglected as well. The temperature dependency of the parameters and the results of the estimation are shown in chapter VI.

### C. Charging - constant voltage phases

In literature the KF is rarely validated during charging. The reason are the slow dynamics in the constant current and voltage phases during the charging process. Because these required informations for the parameter estimator are missing, the estimation can not be precisely. This behaviour is shown for $R_1$ in figure 5. The DKF is initialised with a SOC of 10 %. Due to the missing dynamics mentioned before the parameter is not estimated correctly (from the left to the right). When the

dynamic driving cycle is started more information is available, hence the estimation converges to the measured curve (from the right to the left).

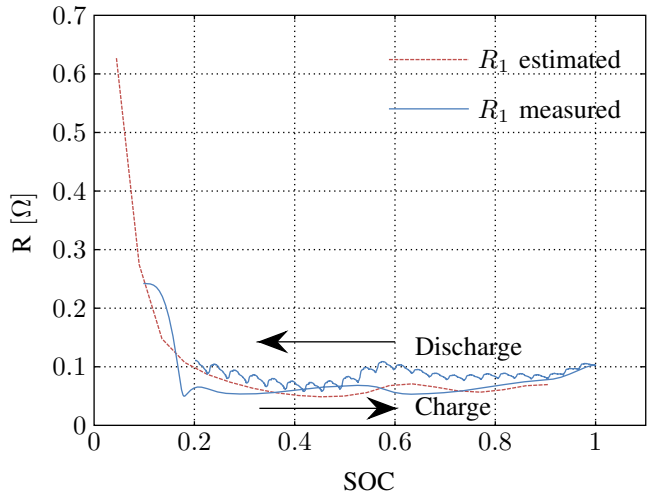


Fig. 5. The measured (red) and the estimated (blue) resistor $R_1$ during charging and discharging

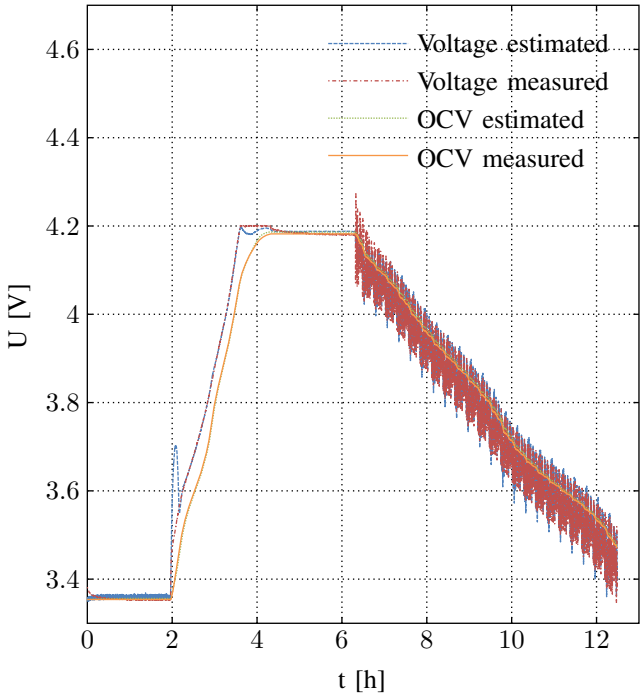


Fig. 6. The measured (red) and estimated (blue) voltage during charging

Considering the voltage estimation (figure 6) an overshoot when the current is switched on can be observed. Thereby the blue curve shows the estimated, the red curve the measured voltage. In the figure also the estimated (green) and measured (orange) OCV is shown. The measured OCV is calculated by the reference SOC and the OCV look up table. The voltage overshoot indicates too high initial parameters of the internal resistances. The DKF is able to correct the parameters quickly. This can be seen in figure 5. In the SOC estimation the overshoot is not visible (figure 7). Also the undershoot of the voltage in the CV phase can arise from the wrong estimation of the parameters during the charging due to missing informations. But the DKF is able to correct the estimation within the constant voltage phase.

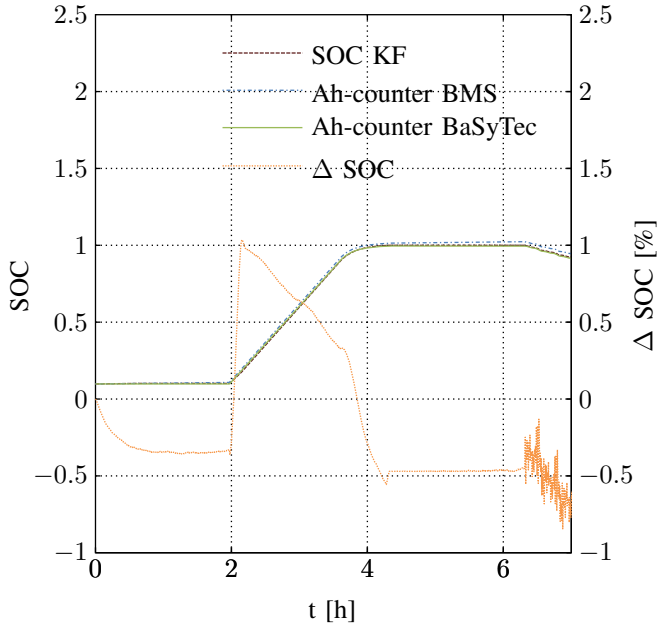


Fig. 7. Behaviour of the state estimator during the less dynamic charging phase

In the literature this problem is often not shown or avoided by using e.g. the inverted driving cycle to charge the cell [11]. Due to this the DKF has enough information also during the charging process.

### *D. Pause - constant SOC phases*

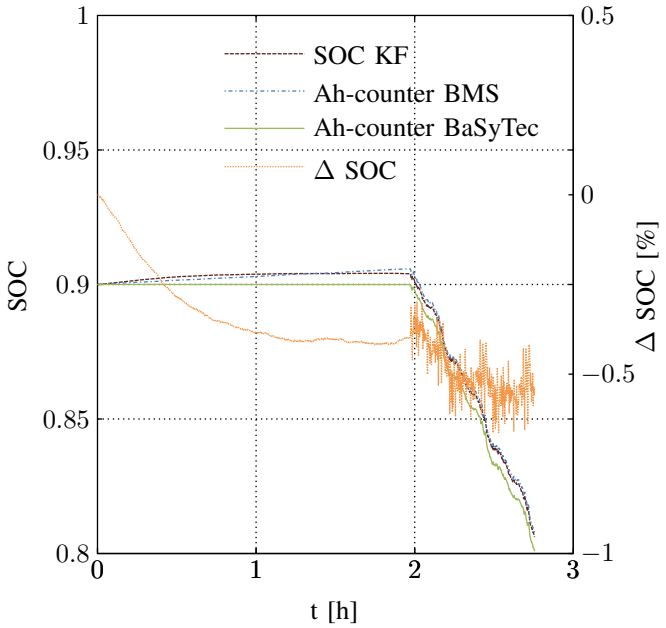


Fig. 8. Two hour pause with the following driving cycle. The DKF corrects the error based on the offset of the current measurement.

Due to the wide measurement range of current sensors the measurement of small currents can be disturbed by noise or the offset of the sensor. This errors can effect the SOC estimation. To investigate this issues long pauses are necessary. During this phase the Ah-counter increases due to the offset of the current sensor, despite of this the SOC estimation of the DKF has to stay constant. Figure 8 shows that after a transient effect the estimated SOC stays constant while the Ah-counter increases the SOC. The transient effects at the beginning are evoked by inaccurate initial parameters. During the driving cycle the estimation converges again to the reference SOC.

### *E. Long term validation*

To prove the stability and the convergence of the DKF a long term validation is necessary. Further investigations have to show the estimation accuracy and the stability of the filter despite variable ambient temperatures and ageing effects. Due to the short term validation in this paper, the capacity $C_N$ is constant.

## V. Design of Experiment

In figure 9 the setting of the experiment is shown. The Artemis driving cycle is applied to the battery with the BaSyTec testing system. In addition the cell voltage and the current are measured with the BMS. The more accurate current sensor from BaSyTec provides the reference SOC. The accuracies of the used sensors are summarised in table III. To conduct the measurements at 5 °C, 25 °C and 35 °C the cell is located in a temperature chamber. In further works temperatures below 0 °C are investigated.

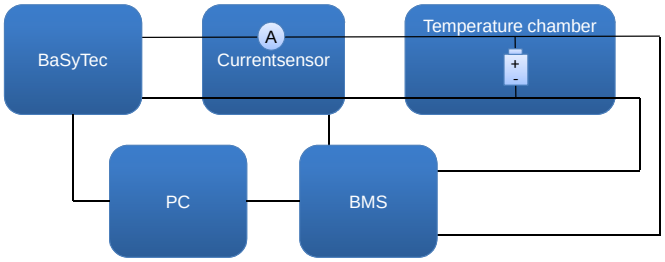


Fig. 9. Design of experiment

| | BaSyTec | BMS |
|---|---|---|
| Voltage resolution | 0.3 mV | 1.5 mV |
| Current resolution | 1 mA | 10 mA |
| Voltage accuracy | 1 mV | ± 0.25 % at 3.6 V |
| Current accuracy | 0.2 mA | ± 0.25 % rdg |

TABLE III. Accuracies of the voltage and current measurement

Based on chapter IV the voltage curve in figure 10 was developed. At the beginning the actual usable capacity is determined by a full CCCV charging followed by a full CCCV discharging. Due to parameter determination problems at low SOCs the battery is pre charged to 10 % where the DKF is initialised. After a pause of two hours the battery is charged to 100 %. Followed a further pause of two hours the discharge is started. Thereby the discharge is a repeating Artemis driving cycle until a defined abort criterion is reached. At the end of the discharge a rest discharge is performed to determine the exact reference SOC. To proof the functionality of the DKF over the hole SOC range the length of the driving cycle is extended about 10 % in every validation cycle. The results from the estimation is compared to the results of the complete discharge test.

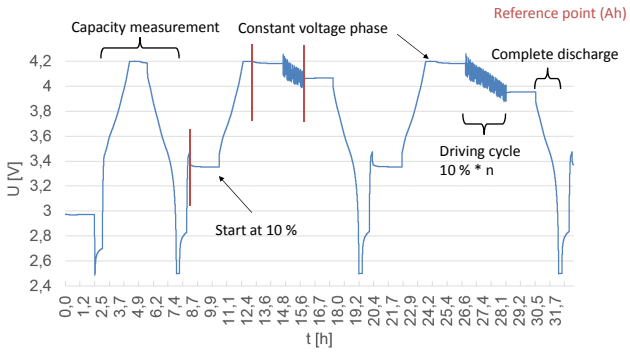


Fig. 10. The validation process

## VI. Results

The estimation results from the DKF compared to the measurements are shown. The reference parameters are determined with current pulses in 5 % steps over the SOC range (chapter II). The reference SOC is determined with the rest discharge test mentioned before. The difference between the measurement and the estimation is indicated with the absolute error in %.

### *A. Temperature influence to the state estimator*

Due to the low dynamic during charging in this paper only the results during discharging are presented. In figure 11 the SOC curve of a discharge with the driving cycle from 90 % to 10 % at 25 °C is shown.

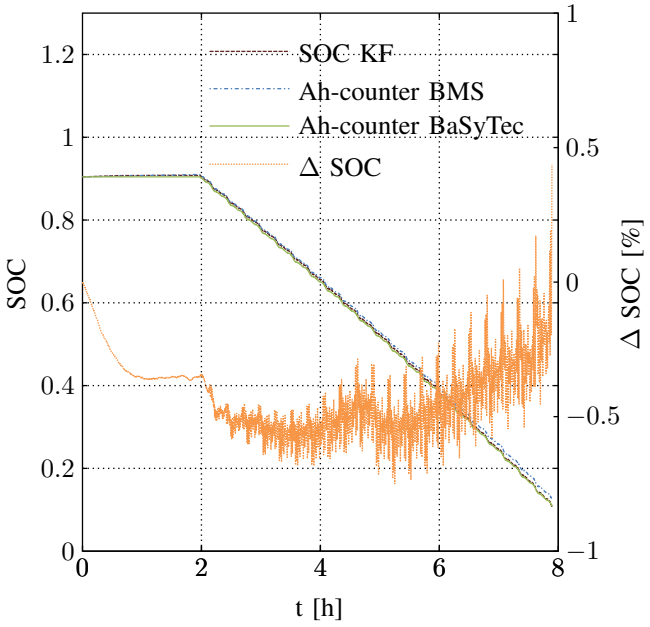


Fig. 11. Comparison of the SOC estimation and the Ah-counter of the BMS and BaSyTec at 25 °C

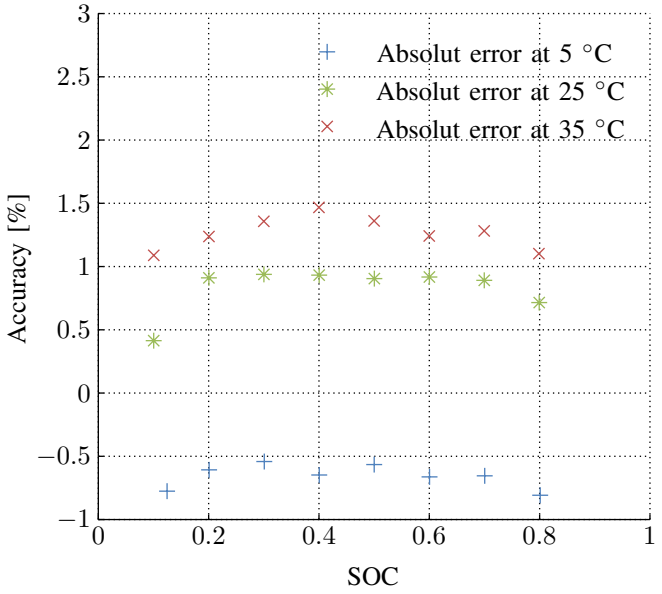


Fig. 12. Results of the state estimation at different SOCs and temperatures

The blue (Ah-counter BMS) curve represents the Ah-counter based on the BMS current sensor. The green (Ah-Counter BaSyTec) curve is the Ah-counter based on the measurement of the BaSyTec test system. The red (SOC KF) curve is the SOC estimation of the DKF and the orange (Δ SOC) curve is the error between the estimation and the reference, respectively. It can be observed that the DKF converges to the reference despite the offset drift of the used current sensor. The noisy error curve (orange) is caused by the asynchronous measurement between the BMS and the BaSyTec. In figure 12 the accuracies of the estimations at the end of every driving cycle and discharge tests are compared. In the range of the tested temperatures the estimation has an absolute accuracy between -1.0 % and +1.5 %. The parallel translation could be induced from the temperature depended OCV. An implementation of the OCV dependency in the model can increase the accuracy.

The results for the resistor $R_{dc1s}$ are shown in figure 13. The measurements and the estimations show a good accordance at different temperatures. Only the estimation at 5 °C shows an underestimation of the resistance.

### *B. Temperature influence to the parameter estimator*

Figure 14 present the results of the RC-term elements. In the measurements of the resistor $R_1$ a low temperature dependency is observable. This is also seen in the estimation. At 25 °C and 35 °C the resistor is under 60 % overestimated, at 5 °C instead underestimated. But the tendency of the curve of the estimation suits to the measurement. The ripple of the estimated resistor arise from the modelling of the process noise. Further investigations have to find a compromise between stability and a dynamic behaviour with respect to reduce the ripple. The validation of the capacity ($C_N$) estimation has to be done in a long term test.

To receive the shown results it was necessary to change the tuning parameters of the DKF at the different temperatures.

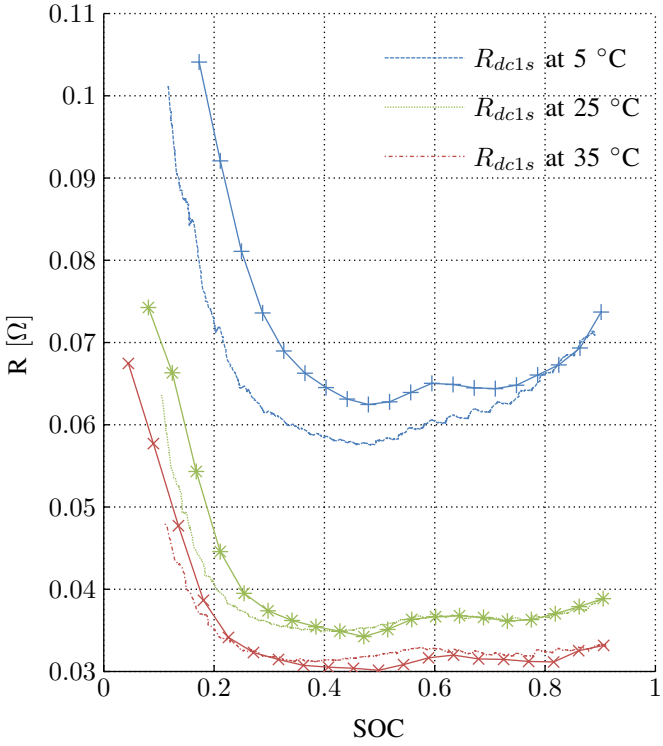


Fig. 13. Estimation of the resistor $R_{dc1s}$ over the SOC range from 90 % to 10 % at different temperatures compared to the measured values (lines with marker)

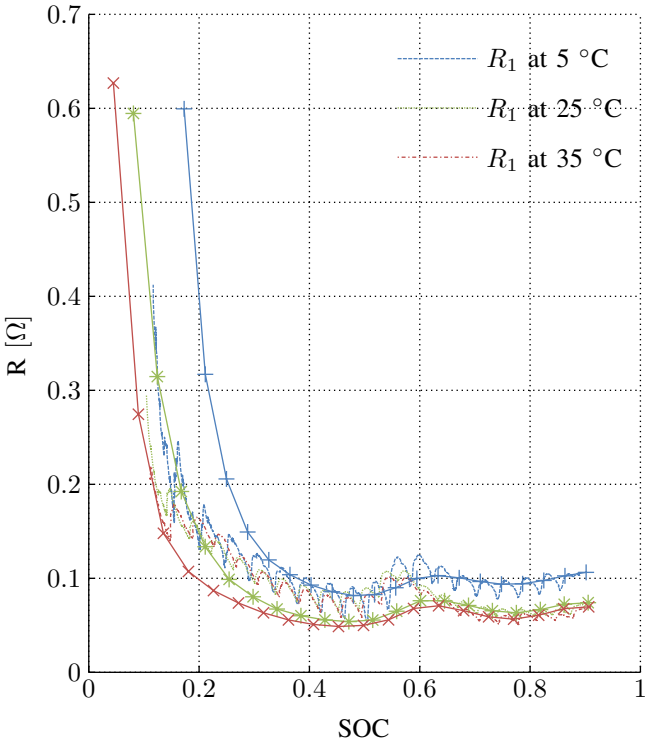


Fig. 14. Estimation of the resistor $R_1$ over the SOC range from 90 % to 10 % at different temperatures compared to the measured values (lines with marker)

## VII. Conclusion

The presented paper shows the validation of a DKF. At the beginning the determination of the reference parameter was shown. The filter structure was explained and the shortcomings of the filter were described. Based on this an objective validation method was illustrated. The validation contains long rest periods, low (charging) and high (driving cycle) dynamic periods. Due to the lower estimation accuracy of the parameters during charging only the result during discharging with the driving cycle were presented. The state estimation shows during discharging at different temperatures an accuracy of 1.5 %. Also the parameter estimation shows a stable behaviour and can follow the measured curves. In further investigations the temperature dependency has to be analysed in more detail, the focus will be on the different results of the state estimator at different temperatures. Furthermore the estimation of the parameters during charging has to be improved.

## Acknowledgment

These results were obtained within the research project FORELMO, which is funded by the Bayrische Forschungsstiftung (BFS).


## References

[1] R. Xiong, X. Gong, C. C. Mi, and F. Sun, "A robust state-of-charge estimator for multiple types of lithium-ion batteries using adaptive extended kalman filter," *Journal of Power Sources*, vol. 243, pp. 805–816, 2013.

[2] M. R. Khan, G. Mulder, and J. van Mierlo, "An online framework for state of charge determination of battery systems using combined system identification approach," *Journal of Power Sources*, vol. 246, pp. 629–641, 2014.

[3] Y. Xing, W. He, M. Pecht, and K. L. Tsui, "State of charge estimation of lithium-ion batteries using the open-circuit voltage at various ambient temperatures," *Applied Energy*, vol. 113, pp. 106–115, 2014.

[4] H. He, R. Xiong, and H. Guo, "Online estimation of model parameters and state-of-charge of lifepo4 batteries in electric vehicles," *Applied Energy*, vol. 89, no. 1, pp. 413–420, 2012.

[5] G. L. Plett, "Extended kalman filtering for battery management systems of lipb-based hev battery packs part 1. background," *Journal of Power Sources*, no. 134, pp. 252–261, 2004.

[6] Walder G., Campestrini C., Lienkamp M., and Jossen A., "Functionality and behaviour of an dual kalman filter implemented on a modular battery-management-system," *Conference on Future Automotive Technology: Focus Electromobility*, 2013.

[7] Christian Linse, "Modellbasierte methoden zur zustandsbestimmung von lithium-ionen-batterien in elektrofahrzeugen: Diplomarbeit," Garching/München, 2011.

[8] G. L. Plett, "Extended kalman filtering for battery management systems of lipb-based hev battery packs part 3. state and parameter estimation," *Journal of Power Sources*, no. 134, pp. 277–292, 2004.

[9] H. Dai, X. Wei, Z. Sun, J. Wang, and W. Gu, "Online cell soc estimation of li-ion battery packs using a dual time-scale kalman filtering for ev applications," *Applied Energy*, vol. 95, pp. 227–237, 2012.

[10] V. V. Viswanathan, D. Choi, D. Wang, W. Xu, S. Towne, R. E. Williford, J.-G. Zhang, J. Liu, and Z. Yang, "Effect of entropy change of lithium intercalation in cathodes and anodes on li-ion battery thermal management," *Journal of Power Sources*, vol. 195, no. 11, pp. 3720–3729, 2010.

[11] J. Lee, O. Nam, and B. Cho, "Li-ion battery soc estimation method based on the reduced order extended kalman filtering," *Journal of Power Sources*, no. 174, pp. 9–15, 2007.